Dark State Engineering in Waveguide QED

R. Holzinger, ¹ R. Gutiérrez-Jáuregui, ² T. Hönigl-Decrinis, ³ G. Kirchmair, ³ A. Asenjo-Garcia, ² and H. Ritsch ¹ Institute for Theoretical Physics, Innsbruck University, Technikerstrasse 21a, 6020 Innsbruck, Austria ² Department of Physics, Columbia University, New York, NY 10027, USA ³ Institute for Quantum Optics and Quantum Information of the Austrian Academy of Sciences, 6020 Innsbruck, Austria (Dated: September 23, 2022)

Subradiant excited states in finite chains of two-level quantum emitters coupled to a one-dimensional reservoir are a resource for superior photon storage and controlled photon manipulation. Typically, states storing multiple excitations exhibit fermionic correlations and are thus characterized by an anti-symmetric wavefunction, which makes them hard to prepare experimentally. Here we identify a special class of quasi-localized dark states with up to half of the qubits excited, which appear for lattice constants that are an integer multiple of the guided-mode wavelength. They allow for a high-fidelity preparation and minimally invasive read out in state-of-the-art setups. In particular, we suggest an experimental implementation using a co-planar wave-guide coupled to superconducting transmon qubits on a chip. As free space and intrinsic losses are minimal, virtually perfect dark states can be achieved even for a low number of qubits, enabling fast preparation and manipulation with high fidelity.

Introduction.—Collective excitation states of ensembles of quantum emitters posses a wealth of surprising physical properties. Typically, the many-body response of these ensembles leads to delocalized excitations that are lost to dissipation at lifetimes that can vary across many different orders of magnitudes. Of particular interest are dark or sub-radiant states whose long life-times can be used to implement extremely efficient quantum memories [1, 2], loss-less transport of photons [3, 4], photon-photon gates [5], to realize future generations of atomic lattice clocks [6, 7] and potentially for improved quantum sensing. Recently, applications towards building superior single photon antennas [8] or nanoscopic coherent or non-classical light sources based on dark resonances were proposed [9].

In most cases, studies and experiments on subradiance focus on manipulating only a single excitation, i.e., they limit their scope to the lowest of the so-called Dicke manifold [9-21]. Many-body subradiant states have attracted more interest only recently, but in general the preparation and manipulation of such states remains challenging as they are typically very delocalized. One option is to use more complex atomic emitters with several internal excited states. This allows to store several photons in a dark subspace, but they are tied to multipartite entanglement, which is fragile in general [22–26]. For a chain of qubits coupled to a waveguide, dark states within the two-excitation sector have been classified into fermionic, dimerized or edge states among others [27–41]. Experimental preparation and control of such states remains challenging and only quite recently the two-excitation sector was probed experimentally with superconducting transmon qubits [42].

In this work, we theoretically predict a new type of many-body dark states that emerge in arrays of qubits coupled to a 1D bath when the lattice constant is an integer of the guided mode wavelength. These dark states are built from antisymmetric superpositions of symmetric states, which are forbidden from decaying into the waveguide. Interestingly, the excitations are strongly localized

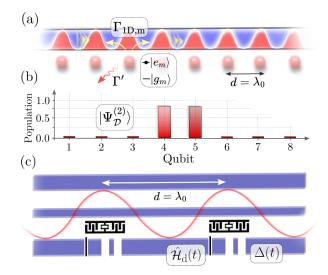


FIG. 1. (a) Schematics of a regular chain of qubits coupled to a 1D waveguide with photon-mediated interactions determined by the single-qubit decay rates $\Gamma_{1D,m}$. For qubits separated by integer multiples of the wavelength λ_0 , a degenerate family of non-radiative dark states forms, which are only subject to very small free space decay Γ' and non-radiative losses. (b) Distribution of the excited state population for N=8 qubits with identical waveguide couplings for a typical two-excitation dark state $|\Psi_{\mathcal{D}}^{(2)}\rangle$ as described by Eq. (7). Two qubits store the major fraction 2(N-3)/(N-2) of the excitation energy. (c) Waveguide QED realization with superconducting circuits: transmons (in black) are coupled to a co-planar waveguide (in blue). The individual qubit frequencies and thus effectively their distance d can be tuned in-situ via flux-bias lines. For the preparation and read-out of dark states, driving pulses $\mathcal{H}_{\rm d}(t)$ and local detuning control $\Delta_{\rm q}(t)$ are applied via separate control lines.

in a small number of the qubits. For instance, we find that the fraction 2(N-2)/N of two excitations in a N qubit array is stored in just two of the qubits, while a vanishing amount of the excitations in the remaining qubits completely inhibits decay into the waveguide, as shown by Fig. 1(b). We show below an analytical description

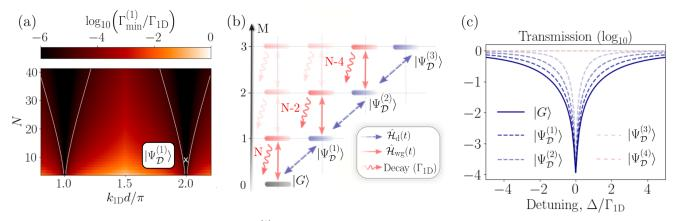


FIG. 2. (a) Minimal excitation decay rate $\Gamma_{\min}^{(1)}$ within the single-excitation sector as a function of qubit number and separation d for lossless qubits with $\Gamma'=0$. The continuous white lines enclose a region of strong collective subradiance, where $\Gamma_{\min}^{(1)}/\Gamma_{1D} \leq 10^{-5}$. The example of Eq. (3) is indicated with a white cross for N=8 qubits. (b) Energy level diagram for the lowest three energy manifolds with arrows indicating the route towards dark state preparation and probing. Coupling to $|\Psi_{\mathcal{D}}^{(M)}\rangle$ is facilitated by a coherent drive $\hat{\mathcal{H}}_{\rm d}(t)$. Once $|\Psi_{\mathcal{D}}^{(M)}\rangle$ is prepared a second field sent through the waveguide, as described by $\hat{\mathcal{H}}_{\rm wg}(t)$ in Eq. (6), transfers the state outside the dark manifold, from where it decays with rate $(N-2M)\Gamma_{\rm 1D}$. (c) Weak field waveguide transmission as a function of probe frequency tuned across the single qubit resonance frequency ω_0 for a 8-qubit chain in the ground state (solid line) and the single- to four-excitation dark states (dashed lines). The blockade window decreases from the linewidth $N\Gamma_{\rm 1D}$ of the symmetric single-excitation state towards $(N-2M)\Gamma_{\rm 1D}$ for the M-excitation dark state and disappears for the four-excitation dark state showing complete transmission.

for these states and characterize their spatial correlations. We also study spectral signatures of photon transport in the presence of these states. Finally, we propose a protocol that allows to store and release the excitations in a controlled fashion.

Model.—The collective dynamics of a chain of qubits resonantly coupled to a 1D waveguide can be described by a master equation [43, 44] of the form $\dot{\hat{\rho}} = -i\left(\hat{\mathcal{H}}_{\text{eff}}\hat{\rho} - \hat{\rho}\hat{\mathcal{H}}_{\text{eff}}^{\dagger}\right) + \sum_{m,n} \Gamma_{m,n}\hat{\sigma}_{m}\hat{\rho}\hat{\sigma}_{n}^{\dagger}$, where $\hat{\sigma}_{m} = |g_{m}\rangle\langle e_{m}|$ is the lowering operator for the mth qubit and $\hbar = 1$. Qubits couple via the waveguide, as described by an effective Hamiltonian that, assuming the Born-Markov approximation, can be written in the interaction picture as

$$\hat{\mathcal{H}}_{\text{eff}} = \sum_{m,n=1}^{N} \left(J_{m,n} - i \frac{\Gamma_{m,n}}{2} \right) \hat{\sigma}_{m}^{\dagger} \hat{\sigma}_{n}, \tag{1}$$

where $J_{m,n} = \sqrt{\Gamma_{1\mathrm{D,m}}\Gamma_{1\mathrm{D,n}}}\sin(k_{1\mathrm{D}}|x_m-x_n|)/2$ and $\Gamma_{m,n} = \sqrt{\Gamma_{1\mathrm{D,m}}\Gamma_{1\mathrm{D,n}}}\cos(k_{1\mathrm{D}}|x_m-x_n|)$ denote the coherent and dissipative interaction terms, respectively. The relative distance between qubit n and m is given by $|x_n-x_m|$, $\Gamma_{1\mathrm{D,n}}$ is the individual decay rate of the qubit n into the waveguide, and $k_{1\mathrm{D}} = \omega_0/c$ is the wavevector of the guided mode on resonance with the qubits. In addition, the qubits experience non-radiative damping Γ' and dephasing, included in the Supplementary Information (SI [45]). Figure 1(a) depicts the system considered in this work with an array of N qubits all separated by a distance d and coupled to a 1D single-mode waveguide. Generally the qubits can exhibit non-identical waveguide couplings. We assume that M qubits are coupled with rate $\Gamma_{1\mathrm{D,1}}$ and N-M qubits with rate $\Gamma_{1\mathrm{D,2}}$. For a qubit separation

 $d = n\lambda_0$ with $n \in \mathbb{N}^+$, the coherent exchange rates in Eq. (1) are zero and only the collective symmetric states of the two parts of the array couple to the waveguide, which allows us to express the effective Hamiltonian as

$$\hat{\mathcal{H}}_{\text{eff}} = -\frac{iM\Gamma_{1D,1}}{2} \mathcal{S}_1^{\dagger} \mathcal{S}_1 - \frac{i(N-M)\Gamma_{1D,2}}{2} \mathcal{S}_2^{\dagger} \mathcal{S}_2 - i\Gamma(\mathcal{S}_1^{\dagger} \mathcal{S}_2 + \mathcal{S}_2^{\dagger} \mathcal{S}_1), \tag{2}$$

with $S_1 = \sum_{j=1}^M \hat{\sigma}_j/\sqrt{M}$ and $S_2 = \sum_{j=M+1}^N \hat{\sigma}_j/\sqrt{N-M}$ being collective symmetric lowering operators. The last term shows that the symmetric superpositions of the two parts of the chain are dissipatively coupled by the enhanced rate $2\Gamma = \sqrt{M(N-M)}\Gamma_{1D,1}\Gamma_{1D,2}$. There are an additional N-1 operators with zero coupling to the waveguide and, therefore, not appearing in Eq. (2). For the sake of clarity we assume identical waveguide couplings from now on and shift the discussion of the general case to the SI [45]. Note that the same results follow for odd multiples of $\lambda_0/2$ separations with the symmetric operators now replaced with anti-symmetric operators, having alternate signs between consecutive qubits.

The case of a single qubit interacting with a chain of qubits in the collective symmetric state can also be realized with two-level atoms in free space. In this analogy the first qubit is placed at the center of a ring of subwavelength-spaced two-level emitters where, due to permutational ring symmetry, only the symmetric mode of the ring couples to the central emitter [46].

Single Excitation.—The qubits decay into the waveguide via collective channels determined by the eigenstates of Eq. (1). For large arrays, the single-excitation eigenstates are approximated by Bloch waves of wavevector k decaying at rates Γ_k [1, 28, 34]. For finite systems,

the decay rates depend on qubit number N and lattice spacing d, as shown in Fig. 2(a) for the slowest decay rate. While in general the decay rate of the most subradiant eigenstate is suppressed with increasing qubit number – following a N^{-3} scaling [28] – this is not the case for spacing $k_{1D}d = n\pi$. In this so-called "mirror configuration" (with $d = n\lambda_0$), there is only one bright state, $|\Psi_S^{(1)}\rangle = (\hat{\sigma}_1^{\dagger} + \sqrt{N-1}S_2^{\dagger})|G\rangle/\sqrt{N}$ where $|G\rangle = |g\rangle^{\otimes N}$, and (N-1) perfectly dark states of exactly zero decay rate.

Leveraging the degeneracy of the dark manifold, one can build highly-localized dark states. Consider the state

$$|\Psi_{\mathcal{D}}^{(1)}\rangle = \frac{1}{\sqrt{N}} \left(\sqrt{N-1}\hat{\sigma}_1^{\dagger} - \hat{\mathcal{S}}_2^{\dagger}\right) |G\rangle, \tag{3}$$

composed of the normalized sum of $|\Psi_m\rangle=1/\sqrt{2}(\hat{\sigma}_1^{\dagger}-\hat{\sigma}_m^{\dagger})|G\rangle$ states spanning the N-1 dark subspace. This dark state bisects the chain into M=1 and N-1 qubits. It displays the unique feature that a large fraction $\langle \hat{\sigma}_1^{\dagger} \hat{\sigma}_1 \rangle = 1 - 1/N$ of the excited state population is concentrated in the first qubit while the remaining qubits share 1/N of the excitation. By increasing the system size, the excitation is mostly stored in the first qubit while being protected from decay by a vanishing amount spread in the remaining qubits.

Dark state preparation and probing.— The choice of storing the excitation in the first qubit is not unique and any other qubit is equally valid [45]. The dark state $|\Psi_{\mathcal{D}}^{(1)}\rangle$, however, can be efficiently prepared by introducing an external coherent drive of frequency ω_l localized on the first qubit. This pulsed drive on resonance with the first qubit couples to the chain via $\hat{\mathcal{H}}_{\rm d}(t) = \Omega_{\rm d}(t)(\hat{\sigma}_1^{\dagger} + \hat{\sigma}_1)$ where $\Omega_{\rm d}(t)$ is a time-dependent Rabi frequency. It connects the ground state to both bright and dark states with asymmetrical coupling strengths

$$\langle \Psi_{\mathcal{S}}^{(1)} | \hat{\mathcal{H}}_{\mathrm{d}}(t) | G \rangle = \Omega_{\mathrm{d}}(t) \sqrt{1/N},$$
 (4)

$$\langle \Psi_{\mathcal{D}}^{(1)} | \hat{\mathcal{H}}_{d}(t) | G \rangle = \Omega_{d}(t) \sqrt{1 - 1/N},$$
 (5)

preparing the dark state with high-fidelity in the $N \gg 1$ limit. The drive not only prepares single-excitation dark states but also connects dark states along the excitation ladder through paths illustrated in Fig. 2(b). These paths continue until half of the qubits are excited and there are no more dark states [35].

To probe the dark states we use a second, weak driving field $(\Omega_{\rm wg}(t)/\Gamma_{\rm 1D}\ll 1)$. The field propagates along the waveguide and couples to the qubits through

$$\hat{\mathcal{H}}_{\text{wg}}(t) = \sum_{j=1}^{N} \left(\Delta_{\text{wg}} \hat{\sigma}_{j}^{\dagger} \hat{\sigma}_{j} + \Omega_{\text{wg}}(t) (\hat{\sigma}_{j}^{\dagger} + \hat{\sigma}_{j}) \right).$$
 (6)

Notice there is no phase pick-up between the qubits due to the $n\lambda_0$ separation. This probe connects dark and bright states through paths shown in Fig. 2(b). It then opens a window into the dark states by measuring the

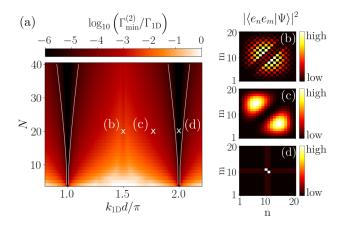


FIG. 3. (a) Minimal decay rate $\Gamma_{\min}^{(2)}$ within the second excitation manifold as a function of chain size N and qubit separation d. The continuous white lines enclose the regions where $\Gamma_{\min}^{(2)}/\Gamma_{1D} \leq 10^{-5}$. The subradiant states generally exhibit non trivial spatial correlations $|\langle e_n e_m | \Psi \rangle|^2$, which renders them challenging to access. For $k_{1D}d = (2n+1)\pi/2$ with $n \in \mathbb{N}$ a checkerboard pattern emerges in (b) whereas in (c) a typical fermionic occupation is shown, which is shared by most subradiant states. In (d) the dark state $|\Psi_D^{(2)}\rangle$, of Eq. (7), is shown for $k_{1D}d = 2n\pi$ with two excitations localized in the center of the array.

field $\hat{E} = \hat{E}_{\rm in} + i\sqrt{\Gamma_{\rm 1D}/2} \sum_j \hat{\sigma}_j$ composed from the superposition of probe and fields scattered into the waveguide. Figure 2(c) shows the transmission $\langle \hat{E}^{\dagger}\hat{E}\rangle/\langle \hat{E}_{\rm in}^{\dagger}\hat{E}_{\rm in}\rangle$ for different initial states. An 8-qubit chain is probed by a rectangular waveguide pulse of duration $t\Gamma_{1D} = 50$ during which the transmitted field is recorded using the master equation accounting for multiple excitations. Note that we assume the ideal case without imperfections and positional disorder which, would lead to a finite lifetime of the dark state and a higher overall transmission. We begin with N qubits in the ground state where the transmission linewidth is $N\Gamma_{1D}$, corresponding to the symmetric state $|\Psi_{\mathcal{S}}^{(1)}\rangle$ excited by the probe. For the qubits prepared in the Mth excitation dark state the transmission linewidth is reduced to $(N-2M)\Gamma_{1D}$ [45]. For a single excitation, with $N \geq 3$, the probe excites $\hat{\mathcal{H}}_{\text{wg}}(t)|\Psi_{\mathcal{D}}^{(1)}\rangle \propto |\Psi^{(2)}\rangle$, with $|\Psi^{(2)}\rangle \propto ((N-2)\sigma_1^{\dagger} - \sqrt{N-1}\mathcal{S}_2^{\dagger}) \mathcal{S}_2^{\dagger}|G\rangle$. For M = N/2the waveguide drive is orthogonal to the dark state and therefore renders the system completely transparent. In this way the two-excitation manifold is utilized to escape the decoherence-free subspace and probe the preparation of the dark state [42].

Multiple Excitations.— The localized dark states for multiple excitations are written explicitly in the SI [45]. For simplicity, we focus on the two-excitation subspace of Eq. (2), where the Hilbert space is spanned by states $|e_n e_m\rangle = \hat{\sigma}_n^{\dagger} \hat{\sigma}_m^{\dagger} |G\rangle$ and the most superradiant two-excitation state can be written as $|\Psi_S^{(2)}\rangle \propto \sum_{j < k} \hat{\sigma}_j^{\dagger} \hat{\sigma}_k^{\dagger} |G\rangle$ with decay rate $2(N-1)\Gamma_{\rm 1D}$. The extension of the dark state in Eq. (3) involving the symmetric operators \mathcal{S}_1 and

 S_2 with M=2 is

$$|\Psi_{\mathcal{D}}^{(2)}\rangle = \frac{\sqrt{N-3}}{\sqrt{N-1}} \left((\mathcal{S}_1^{\dagger})^2 - \frac{\sqrt{2}\mathcal{S}_1^{\dagger}\mathcal{S}_2^{\dagger}}{\sqrt{N-2}} + \frac{(\mathcal{S}_2^{\dagger})^2}{N-3} \right) |G\rangle, (7)$$

with 2(N-3)/(N-2) of the two excitations stored in the first two qubits. Note that there are N(N-1)/2 combinations of qubit pairs that are equally valid to form S_1 .

The advantage and special nature of the "mirror configuration" (of lattice constant close or equal to $n\lambda_0$) is illustrated in Fig. 3. Figure 3(a) shows the minimal decay rate $\Gamma_{\min}^{(2)}$ as a function of qubit number N and relative distance d. Qualitatively different spatial correlations $|\langle e_n e_m | \Psi \rangle|^2$ of different types of dark states are shown in Figs. 3(b)-(c). For $k_{1D}d = (2n+1)\pi/2$ with $n \in \mathbb{N}$, the correlations display a checkerboard-type pattern [28] due to the fact that the coherent nearest-neighbor and dissipative next-nearest-neighbour interactions in Eq. (1) are zero. Figure 3(c) shows a typical state, described by a fermionic Ansatz, where two-excitation states are composed of single-excitation subradiant states, commonly found as well for multiple excitations [1, 27]. For a large number of qubits, $N \gtrsim 50$ and $k_{1D}d = (6n-1)\pi/6$, another extremely subradiant two-excitation state emerges with dimerized spatial correlations and a decay rate lower than any fermionic-type state [30]. In Fig. 3(d), the correlations for the dark state $|\Psi_{\mathcal{D}}^{(2)}\rangle$ with $k_{1D}d = 2\pi n$ are shown and the exact form is depicted in Eq. (7) with the majority of two excitations stored in just two gubits (in the case of Fig. 3(d) the central two qubits of a 20-qubit chain).

The spatial correlations of the dark state lead to easily accessible preparation as opposed to most other subradiant states with non-trivial spatial correlations. For instance, a (local) coherent drive with Rabi frequency $\Omega_{\rm d}(t)$ exciting two of the qubits drives the dark state with strength $\Omega_{\rm d}(t)\sqrt{N-3}/\sqrt{N-1}$ and subsequently a waveguide drive can be used to probe the preparation of the dark state, see also Fig. 2(b). The transmission in Fig. 2(c) shows a reduction in linewidth if the dark state $|\Psi_{\mathcal{D}}^{(M)}\rangle$ is prepared compared to $N\Gamma_{1D}$ if all qubits are in the ground state, due to the fact that the waveguide drive in Eq. (6) excites the dark state to M+1 excitation states exhibiting decay rates $(N-2M)\Gamma_{1D}$ into the waveguide [45]. As a consequence for N being odd or even, the N/2 or (N-1)/2 excitation dark state leads to unit transmission.

Two-Photon Storage and Release.—Building on the above results we establish a simple protocol for storing and releasing two excitations into the waveguide. Starting with N qubits in the ground state a coherent pulse on the first two qubits prepares the dark state $|\Psi_{\mathcal{D}}^{(2)}\rangle$. The two excitations can now be stored for a time τ after which the last N-2 qubits are detuned by $\Delta_{\mathbf{q}} \gtrsim (N-2)\Gamma_{1D}$, which transfers most of the two excitations to the product state $|e_1e_2\rangle$. This is illustrated in Fig. 4 for a 16-qubit chain

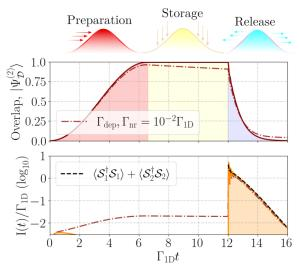


FIG. 4. Preparation, storage and release of two excitations for a 16-qubit chain with multiple of λ_0 separation between the qubits. A π -pulse of Gaussian temporal profile with Rabi frequency $0.25\Gamma_{1D}$, duration $8\Gamma_{1D}$ at the FWHM, and maximum intensity at $t_0 = 3\Gamma_{1D}^{-1}$ drives the first two qubits preparing the dark state $|\Psi_{\mathcal{D}}^{(2)}\rangle$. Subsequently the two excitations are stored for a time $\tau\Gamma_{1D} \approx 5.8$ and released superradiantly by detuning the last N-2 qubits by $\Delta_{\rm q}/\Gamma_{\rm 1D}=50$. The dasheddotted line shows the effect of individual qubit dephasing and non-radiative decay for comparison to the ideal case. The emission is shown via the radiated instensity of the electric field $I(t) = \langle \hat{E}^{\dagger} \hat{E} \rangle (t)$ into the waveguide and exhibits a sharp intensity pulse after the detuning is turned on, whereas during the preparation and storage the emission is negligible. The emission including imperfections is shown in red and the dashed black line shows that the emission process is well approximated by neglecting the interference term $2\text{Re}\langle S_1^{\dagger} S_2 \rangle$.

where a coherent drive $\hat{\mathcal{H}}_{d}(t) = \Omega_{d}(t)(\hat{\sigma}_{1}^{\dagger} + \hat{\sigma}_{2}^{\dagger} + h.c.)$ prepares the state $|\Psi_{\mathcal{D}}^{(2)}\rangle$ with and without imperfections. At $\Gamma_{1D}t = 12$ the last 14 qubits are detuned by $\Delta_{q} = 50\Gamma_{1D}$ from the resonance frequency ω_0 which initiates decay of the excitations. The radiated intensity $I(t) = \langle \hat{E}^{\dagger} \hat{E} \rangle (t)$, equivalently expressed as $\langle S_1^{\dagger} S_1 \rangle + \langle S_2^{\dagger} S_2 \rangle + 2 \operatorname{Re} \langle S_1^{\dagger} S_2 \rangle$ is shown as well with a sharp pulse of emission appearing after the detuning is turned on. The detuning essentially reduces the last term, upon which the two parts of the qubit chain decay independently with initial rates $2\Gamma_{1D}$ and $2(N-3)\Gamma_{1D}$ respectively. Notably the protocol can be extended to M excitations which are stored in the dark state $|\Psi^{(M)}_{\mathcal{D}}\rangle$ and after detuning the last N-Mqubits, the excitations are emitted superadiantly into the waveguide with peak emission rate $\propto M^2\Gamma_{1D}$ [1, 34]. Superconducting circuit implementation.—Due to nearperfect mode matching, superconducting qubits in a 1D transmission line [10, 47–49] are an ideal platform for realizing this work. Here, we focus on the implementation with transmon gubits capacitively coupled to a common co-planar waveguide as shown schematically in Fig. 1(c). Similar to Ref. [50], the distance d between the qubits on chip is fixed but changing the frequency at which the

transmon qubits emit effectively changes their separation. This ensures that we can satisfy $d \sim \lambda_0$, as well as tune qubits on and off resonance via on-chip flux lines. Weakly-coupled control lines realize the drive $\hat{\mathcal{H}}_{\rm d}(t)$ and allow to selectively excite the single qubits respectively in-situ, and thus prepare dark states [42]. Non-radiative decay rates $\Gamma_{\rm nr}$ and dephasing rates $\Gamma_{\rm dep}$ for superconducting qubits are usually multiple orders of magnitude smaller than typical couplings to the waveguide $\Gamma_{\rm 1D,m}$ [45]. The achievable parameters are easily sufficient to realize the protocol demonstrated in Fig. 4 with high fidelity.

Conclusions. — Motivated by state of the art implementations of waveguide-coupled superconducting qubits, we introduced and studied a theoretical model of the properties and excitation pathways of multi-excitation dark states. Due to the symmetry and (practically infiniterange) all to all coupling, such system possesses almost degenereate manifolds of multi-excitation states radiatively decoupled from the waveguide if the qubits are positioned at wavelength distance. These states allow to absorb and store multiple photons simultaneously [45], while localizing the majority of the excitation energy in just a handful of gubits. This contrasts with typical free space subradiant states, where each excitation is maximally delocalized. Their localized nature facilitates the preparation of these states via local addressing of individual qubits, which is currently available in state of the art implementations. As the system also allows for controlled release of all energy into the waveguide, possible applications point towards non-classical multi-photon sources or a tailored memory for a quantum repeater. As the projected numbers for experimental realizations seem favorable, we expect to inspire efforts in various quantum simulation platforms including superconducting circuits or Rydberg arrays [7, 51]. Similarly, optical waveguide systems [14] and atoms, which are tweezer trapped in optical resonators, can be envisaged [52] as an alternative setup once a suitable long wavelength transition is identified. This system can also be used as an analog simulator to mimic the properties of highly symmetric quantum emitter arrays as e.g. coupled ring structures, which play a central role in biological light harvesting systems and are too complex for numerical simulations [53].

R.H. and H.R. acknowledge funding from the Austrian Science Fund (FWF) doctoral college DK-ALM W1259-N27 and the FET OPEN Network Cryst3 funded by the European Union (EU) via Horizon 2020. T. H-D. acknowledges financial support from the Lise Meitner programme of the Austrian Science Fund (FWF), project M3347. AAG gratefully acknowledges support from the Air Force Office of Scientific Research through their Young Investigator Prize (grant No. 21RT0751), the National Science Foundation through their CAREER Award (No. 2047380), the A. P. Sloan foundation, and the David and Lucile Packard foundation. G.K. acknowledges funding by the European Research Council (ERC) under the European Union's Horizon 2020 research and innovation program (714235).

- A. Asenjo-Garcia, M. Moreno-Cardoner, A. Albrecht, H. J. Kimble, and D. E. Chang, "Exponential improvement in photon storage fidelities using subradiance and "selective radiance" in atomic arrays," Phys. Rev. X 7, 031024 (2017).
- [2] M. Moreno-Cardoner, D. Plankensteiner, L. Ostermann, D. E. Chang, and H. Ritsch, "Subradiance-enhanced excitation transfer between dipole-coupled nanorings of quantum emitters," Phys. Rev. A 100, 023806 (2019).
- [3] S. J. Masson and A. Asenjo-Garcia, "Atomic-waveguide quantum electrodynamics," Phys. Rev. Research 2, 043213 (2020).
- [4] R. Gutiérrez-Jáuregui and A. Asenjo-Garcia, "Directional transport along an atomic chain," Phys. Rev. A 105, 043703 (2022).
- [5] M. Moreno-Cardoner, D. Goncalves, and D. E. Chang, "Quantum nonlinear optics based on two-dimensional rydberg atom arrays," Phys. Rev. Lett. 127, 263602 (2021).
- [6] I. S. Madjarov, A. Cooper, A. L. Shaw, J. P. Covey, V. Schkolnik, T. H. Yoon, J. R. Williams, and M. Endres, "An atomic-array optical clock with single-atom readout," Phys. Rev. X 9, 041052 (2019).
- [7] M. A. Norcia, A. W. Young, W. J. Eckner, E. Oelker, J. Ye, and A. M. Kaufman, "Secondsscale coherence on an optical clock transition in a tweezer array," Science 366, 93–97 (2019), https://www.science.org/doi/pdf/10.1126/science.aay0644.
- [8] M. Moreno-Cardoner, R. Holzinger, and H. Ritsch, "Ef-

- ficient nano-photonic antennas based on dark states in quantum emitter rings," Opt. Express **30**, 10779–10791 (2022).
- [9] R. Holzinger, M. Moreno-Cardoner, and H. Ritsch, "Nanoscale continuous quantum light sources based on driven dipole emitter arrays," Applied Physics Letters 119, 024002 (2021).
- [10] M. Mirhosseini, E. Kim, X. Zhang, A. Sipahigil, P. B. Dieterle, A. J. Keller, A. Asenjo-Garcia, D. E. Chang, and O. Painter, "Cavity quantum electrodynamics with atom-like mirrors," Nature 569, 692–697 (2019).
- [11] M. T. Manzoni, M. Moreno-Cardoner, A. Asenjo-Garcia, J. V. Porto, A. V. Gorshkov, and D. E. Chang, "Optimization of photon storage fidelity in ordered atomic arrays," New Journal of Physics 20, 083048 (2018).
- [12] K. E. Ballantine and J. Ruostekoski, "Quantum single-photon control, storage, and entanglement generation with planar atomic arrays," PRX Quantum 2, 040362 (2021).
- [13] D. F. Kornovan, N. V. Corzo, J. Laurat, and A. S. Sheremet, "Extremely subradiant states in a periodic one-dimensional atomic array," Phys. Rev. A 100, 063832 (2019).
- [14] N. V. Corzo, J. Raskop, A. Chandra, A. S. Sheremet, B. Gouraud, and J. Laurat, "Waveguide-coupled single collective excitation of atomic arrays," Nature 566, 359– 362 (2019).
- [15] B. Olmos, G. Buonaiuto, P. Schneeweiss, and

- I. Lesanovsky, "Interaction signatures and non-gaussian photon states from a strongly driven atomic ensemble coupled to a nanophotonic waveguide," Phys. Rev. A 102, 043711 (2020).
- [16] T. Orell, M. Zanner, M. L. Juan, A. Sharafiev, R. Albert, S. Oleschko, G. Kirchmair, and M. Silveri, "Collective bosonic effects in an array of transmon devices," Phys. Rev. A 105, 063701 (2022).
- [17] X.-L. Chu, V. Angelopoulou, P. Lodahl, and N. Rotenberg, "Sub-radiant states for imperfect quantum emitters coupled by a nanophotonic waveguide," (2022).
- [18] Y. He, L. Ji, Y. Wang, L. Qiu, J. Zhao, Y. Ma, X. Huang, S. Wu, and D. E. Chang, "Geometric control of collective spontaneous emission," Phys. Rev. Lett. 125, 213602 (2020).
- [19] O. Rubies-Bigorda, V. Walther, T. L. Patti, and S. F. Yelin, "Photon control and coherent interactions via lattice dark states in atomic arrays," Phys. Rev. Research 4, 013110 (2022).
- [20] R. J. Bettles, S. A. Gardiner, and C. S. Adams, "Cooperative eigenmodes and scattering in one-dimensional atomic arrays," Phys. Rev. A 94, 043844 (2016).
- [21] V. Paulisch, H. J. Kimble, and A. González-Tudela, "Universal quantum computation in waveguide QED using decoherence free subspaces," New Journal of Physics 18, 043041 (2016).
- [22] A. Asenjo-Garcia, H. J. Kimble, and D. E. Chang, "Optical waveguiding by atomic entanglement in multilevel atom arrays," Proceedings of the National Academy of Sciences 116, 25503–25511 (2019), https://www.pnas.org/doi/pdf/10.1073/pnas.1911467116.
- [23] A. González-Tudela, V. Paulisch, H. J. Kimble, and J. I. Cirac, "Efficient multiphoton generation in waveguide quantum electrodynamics," Phys. Rev. Lett. 118, 213601 (2017).
- [24] R. Holzinger, L. Ostermann, and H. Ritsch, "Subradiance in multiply excited states of dipole-coupled v-type atoms," EPL (Europhysics Letters) 128, 44001 (2020).
- [25] O. Rubies-Bigorda, S. Ostermann, and S. F. Yelin, "Generating multi-excitation subradiant states in incoherently excited atomic arrays," (2022).
- [26] Q.-M. Chen, Y.-x. Liu, L. Sun, and R.-B. Wu, "Tuning the coupling between superconducting resonators with collective qubits," Phys. Rev. A 98, 042328 (2018).
- [27] Y.-X. Zhang and K. Mølmer, "Theory of subradiant states of a one-dimensional two-level atom chain," Phys. Rev. Lett. 122, 203605 (2019).
- [28] A. Albrecht, L. Henriet, A. Asenjo-Garcia, P. B. Dieterle, O. Painter, and D. E. Chang, "Subradiant states of quantum bits coupled to a one-dimensional waveguide," New Journal of Physics 21, 025003 (2019).
- [29] L. Henriet, J. S. Douglas, D. E. Chang, and A. Albrecht, "Critical open-system dynamics in a one-dimensional optical-lattice clock," Phys. Rev. A 99, 023802 (2019).
- [30] Y.-X. Zhang, C. Yu, and K. Mølmer, "Subradiant bound dimer excited states of emitter chains coupled to a one dimensional waveguide," Phys. Rev. Research 2, 013173 (2020).
- [31] B. Bakkensen, Y.-X. Zhang, J. Bjerlin, and A. S. Sørensen, "Photonic bound states and scattering resonances in waveguide qed," (2021).
- [32] Y.-L. L. Fang, H. Zheng, and H. U. Baranger, "Onedimensional waveguide coupled to multiple qubits: photon-photon correlations," EPJ Quantum Technology

- **1**, 3 (2014).
- [33] J. Zhong, N. A. Olekhno, Y. Ke, A. V. Poshakinskiy, C. Lee, Y. S. Kivshar, and A. N. Poddubny, "Photonmediated localization in two-level qubit arrays," Phys. Rev. Lett. 124, 093604 (2020).
- [34] A. S. Sheremet, M. I. Petrov, I. V. Iorsh, A. V. Poshakinskiy, and A. N. Poddubny, "Waveguide quantum electrodynamics: collective radiance and photon-photon correlations," (2021), arXiv:2103.06824 [quant-ph].
- [35] A. V. Poshakinskiy and A. N. Poddubny, "Dimerization of many-body subradiant states in waveguide quantum electrodynamics," Phys. Rev. Lett. 127, 173601 (2021).
- [36] A. V. Poshakinskiy, J. Zhong, Y. Ke, N. A. Olekhno, C. Lee, Y. S. Kivshar, and A. N. Poddubny, "Quantum hall phases emerging from atom-photon interactions," npj Quantum Information 7, 34 (2021).
- [37] S. D. Jenkins, J. Ruostekoski, N. Papasimakis, S. Savo, and N. I. Zheludev, "Many-body subradiant excitations in metamaterial arrays: Experiment and theory," Phys. Rev. Lett. 119, 053901 (2017).
- [38] Y. Ke, A. V. Poshakinskiy, C. Lee, Y. S. Kivshar, and A. N. Poddubny, "Inelastic scattering of photon pairs in qubit arrays with subradiant states," Phys. Rev. Lett. 123, 253601 (2019).
- [39] S. J. Masson, I. Ferrier-Barbut, L. A. Orozco, A. Browaeys, and A. Asenjo-Garcia, "Many-body signatures of collective decay in atomic chains," Phys. Rev. Lett. 125, 263601 (2020).
- [40] N. Fayard, L. Henriet, A. Asenjo-Garcia, and D. E. Chang, "Many-body localization in waveguide quantum electrodynamics," Phys. Rev. Research 3, 033233 (2021).
- [41] J. Zhong and A. N. Poddubny, "Classification of threephoton states in waveguide quantum electrodynamics," Phys. Rev. A 103, 023720 (2021).
- [42] M. Zanner, T. Orell, C. M. F. Schneider, R. Albert, S. Oleschko, M. L. Juan, M. Silveri, and G. Kirchmair, "Coherent control of a multi-qubit dark state in waveguide quantum electrodynamics," Nature Physics 18, 538–543 (2022).
- [43] K. Lalumière, B. C. Sanders, A. F. van Loo, A. Fedorov, A. Wallraff, and A. Blais, "Input-output theory for waveguide qed with an ensemble of inhomogeneous atoms," Phys. Rev. A 88, 043806 (2013).
- [44] D. E. Chang, L. Jiang, A. V. Gorshkov, and H. J. Kimble, "Cavity QED with atomic mirrors," New Journal of Physics 14, 063003 (2012).
- [45] "See supplemental material at," URL_will_be_inserted_by_publisher (.), for a general description of the M-excitation dark state, the dynamics between the bright-and dark state manifolds, the effect of positional disorder, imperfections and the multilevel nature of the transmon.
- [46] R. Holzinger, D. Plankensteiner, L. Ostermann, and H. Ritsch, "Nanoscale coherent light source," Phys. Rev. Lett. 124, 253603 (2020).
- [47] O. Astafiev, A. M. Zagoskin, A. A. Abdumalikov, Y. A. Pashkin, T. Yamamoto, K. Inomata, Y. Nakamura, and J. S. Tsai, "Resonance fluorescence of a single artificial atom," Science 327, 840–843 (2010).
- [48] T. Hönigl-Decrinis, R. Shaikhaidarov, S. de Graaf, V. Antonov, and O. Astafiev, "Two-level system as a quantum sensor for absolute calibration of power," Phys. Rev. Applied 13, 024066 (2020).
- [49] J. D. Brehm, R. Gebauer, A. Stehli, A. N. Poddubny, O. Sander, H. Rotzinger, and A. V. Ustinov, "Slowing

down light in a qubit metamaterial," (2022).

- [50] A. F. van Loo, A. Fedorov, K. Lalumière, B. C. Sanders, A. Blais, and A. Wallraff, "Photon-mediated interactions between distant artificial atoms," Science 342, 1494–1496 (2013).
- [51] E. Kuznetsova, S. T. Rittenhouse, H. R. Sadeghpour, and S. F. Yelin, "Rydberg-atom-mediated nondestructive readout of collective rotational states in polar-molecule arrays," Phys. Rev. A 94, 032325 (2016).
- [52] N. Sauerwein, F. Orsi, P. Uhrich, S. Bandyopadhyay,
- F. Mattiotti, T. Cantat-Moltrecht, G. Pupillo, P. Hauke, and J.-P. Brantut, "Engineering random spin models with atoms in a high-finesse cavity," (2022).
- [53] A. Potočnik, A. Bargerbos, F. A. Y. N. Schröder, S. A. Khan, M. C. Collodo, S. Gasparinetti, Y. Salathé, C. Creatore, C. Eichler, H. E. Türeci, A. W. Chin, and A. Wallraff, "Studying light-harvesting models with superconducting circuits," Nature Communications 9, 904 (2018).

Appendix A: M-Excitation Dark State

Similar to the single excitation dark state $|\Psi_{\mathcal{D}}^{(1)}\rangle$ in the main text the two-excitation dark state can be decomposed into a sum of (N-2)(N-3)/6 dark states. Defining the state $|\Psi_{ij}\rangle = ((\mathcal{S}_{nm}^{\dagger})^2 + (\mathcal{S}_{ij}^{\dagger})^2 - \mathcal{S}_{nm}^{\dagger}\mathcal{S}_{ij}^{\dagger})|G\rangle$, where $\mathcal{S}_{ij}^{\dagger} = (\hat{\sigma}_i^{\dagger} + \hat{\sigma}_j^{\dagger})/\sqrt{2}$ and $\mathcal{S}_{nm}^{\dagger} = (\hat{\sigma}_n^{\dagger} + \hat{\sigma}_m^{\dagger})/\sqrt{2}$, we can write

$$|\Psi_{\mathcal{D}}^{(2)}\rangle = \sqrt{\frac{2}{(N-2)(N-3)}} \sum_{i < j; i, j \neq n, m}^{N} |\Psi_{ij}\rangle.$$
 (A1)

Given a linear chain of N qubits at multiples of λ_0 separation coupled to a 1D waveguide we proceed with the generalization of the dark state presented in the main text to M excitations, given $M \leq N/2$. Assuming identical waveguide couplings Γ_{1D} for all qubits, the single- and two-excitation dark states can be extended to arbitrary excitations by using the condition that it has to be a combination of the symmetric operators $\mathcal{S}_1^\dagger = \sum_{j=1}^M \hat{\sigma}_j^\dagger/\sqrt{M}$ and $\mathcal{S}_2^\dagger = \sum_{j=M+1}^N \hat{\sigma}_j^\dagger/\sqrt{N-M}$, namely $c_k(\mathcal{S}_1^\dagger)^{M-k}(\mathcal{S}_2^\dagger)^k$, with $k \in \{0,...,M\}$. Consequently the eigenvalue equation $\hat{\mathcal{H}}_{\mathrm{eff}}|\Psi_{\mathcal{D}}^{(M)}\rangle = 0|\Psi_{\mathcal{D}}^{(M)}\rangle$ leads to a system of M+1 equations, which can be solved. Alternatively the Gram-Schmidt procedure can be applied with the initial eigenstate being the symmetric M-excitation eigenstate up to normalization $|\Psi_{\mathcal{S}}^{(M)}\rangle \propto (\sqrt{M}\mathcal{S}_1^\dagger + \sqrt{N-M}\mathcal{S}_2^\dagger)^M|G\rangle$ with decay rate $\Gamma_{\mathcal{S}} = M(N-M+1)\Gamma_{1D}$. The general expression for the M-excitation dark state reads

$$\left|\Psi_{\mathcal{D}}^{(M)}\right\rangle = \sqrt{\frac{(N-2M+1)!(N-2M)!}{(N-M+1)!(N-M)!}} \sum_{k=0}^{M} (-1)^k \binom{N-M-k}{M-k} \left[\sqrt{M}\mathcal{S}_1^{\dagger}\right]^{M-k} \left[\sqrt{N-M}\mathcal{S}_2^{\dagger}\right]^k \left|G\right\rangle. \tag{A2}$$

This is the unique dark state which involves the operators S_1 , S_2 and is orthogonal to $|\Psi_S^{(M)}\rangle$. The cases for M=1,2 are already shown in the main text, the dark state for M=3 excitations is given by

$$\left|\Psi_{\mathcal{D}}^{(3)}\right\rangle = \sqrt{\frac{N-5}{N-2}} \left[\frac{\sqrt{3}(\mathcal{S}_{1}^{\dagger})^{3}}{2} - \frac{3(\mathcal{S}_{1}^{\dagger})^{2}\mathcal{S}_{2}^{\dagger}}{2\sqrt{N-3}} + \frac{\sqrt{3}\mathcal{S}_{1}^{\dagger}(\mathcal{S}_{2}^{\dagger})^{2}}{N-4} - \frac{\sqrt{N-3}(\mathcal{S}_{2}^{\dagger})^{3}}{(N-4)(N-5)} \right] \left| G \right\rangle. \tag{A3}$$

Given the expression for the M-excitation dark state, the excited state population in the first M qubits is expressed as

$$\sum_{j=1}^{M} \langle \Psi_{\mathcal{D}}^{(M)} | \hat{\sigma}_{j}^{\dagger} \hat{\sigma}_{j} | \Psi_{\mathcal{D}}^{(M)} \rangle = \frac{N - 2M + 1}{N - 2M + 2}.$$
 (A4)

The choice of letting the first M qubits be excited is arbitrary as, for a qubit separation of multiples of λ_0 , any M of the N qubits can be excited in order to prepare the dark state $|\Psi_{\mathcal{D}}^{(M)}\rangle$. Also, by letting the distace be odd multiples of $\lambda_0/2$, the same results as above hold, in which case the symmetric operators are replaced by anti-symmetric operators with alternating sign between consecutive qubits.

One more note on the orthogonality of the single-excitation dark state $|\Psi_{\mathcal{D}}^{(1)}\rangle$ of the main text: let us define another equally valid dark state $|\tilde{\Psi}_{\mathcal{D}}^{(1)}\rangle = 1/\sqrt{N}(\sqrt{N-1}\hat{\sigma}_N^{\dagger} - \mathcal{S}_2^{\dagger})|G\rangle$, where \mathcal{S}_2^{\dagger} creates the symmetric superposition for the first N-1 qubits. It follows that these two dark states are nearly orthogonal for large N, namely, $|\langle \tilde{\Psi}_{\mathcal{D}}^{(1)} | \Psi_{\mathcal{D}}^{(1)} \rangle| = 1/(N-1)$.

Appendix B: Bright/Dark Subspaces

In this section we explain the possible excitation/decay paths for the highly degenerate effective Hamiltonian at multiples of λ_0 qubit separation in more detail, in particular to understand the transmission properties if a certain dark state is prepared. Using the language of Dicke superradiance for collective spins, the symmetric collapse operator for all qubits, $\mathcal{S} = (\sqrt{M}\mathcal{S}_1 + \sqrt{N-M}\mathcal{S}_2)/\sqrt{N}$ is in the angular momentum representation for the sum of N spin 1/2 subsystems and defines lowering/raising operations on the Dicke states, $\mathcal{S}|N/2,m\rangle \propto |N/2,m-1\rangle$ and $\mathcal{S}^{\dagger}|N/2,m\rangle \propto |N/2,m+1\rangle$ where states are generally expressed as $|m,s\rangle$ with the quantum numbers s running from 0 or 1/2 to N/2 and m from -s to s. The Dicke states are explicitly given by the symmetric M-excitation states $|\Psi_{\mathcal{S}}^{(M)}\rangle$ with a decay rates $M(N-M+1)\Gamma_{1D}$ and are shown in Fig. 5. There are additional bright states, for instance $|N/2-1,m\rangle$ with a (N-1)-fold degeneracy and decay rates $(M-1)(N-M)\Gamma_{1D}$.

For multiples of λ_0 separation, the Dicke limit, jumps between different excitation manifolds can only be achieved with the symmetric operator \mathcal{S} and a waveguide drive on resonance with the qubit transition frequency ω_0 that excites all qubits equally can be expressed as

$$\hat{\mathcal{H}}_{\text{wg}}(t) = \Omega_{\text{wg}}(t) \left(\sqrt{M} \mathcal{S}_1^{\dagger} + \sqrt{N - M} \mathcal{S}_2^{\dagger} + h.c. \right), \tag{B1}$$

where the qubit chain is partitioned into M and N-M qubit arrays respectively, and $\Omega_{\rm d}(t)$ is the time dependent Rabi frequency which can be pulsed or continuous. The waveguide drive can now connect Dicke states with the same quantum number m shown as vertical red arrows in Fig. 5 but is not able to access the completely dark state manifold which requires some asymmetry that is provided here by a coherent drive on a single or multiple qubits, $\hat{\mathcal{H}}_{\mathrm{d}}(t) = \Omega_{\mathrm{d}}(t) \sum_{m} (\hat{\sigma}_{m}^{\dagger} + \hat{\sigma}_{m})$, with the requirement that only up to N-1 qubits are driven, in order to have non-zero overlap with the dark state manifold. This way, the every dark state (up to the N/2-excitation manifold) can be driven. Alternatively, the single-excitation dark state $|\Psi_{\mathcal{D}}^{(1)}\rangle$ can be prepared by driving a single qubit, subsequently $|\Psi_{\mathcal{D}}^{(2)}\rangle$ can be prepared by driving another qubit and so on up to $|\Psi_{\mathcal{D}}^{(N/2)}\rangle$ as shown in Fig. 5. On the other hand, for instance, the waveguide drive in Eq. (B1) drives the single-excitation dark state $|\Psi_{\mathcal{D}}^{(1)}\rangle$ to the two-excitation bright state

$$|\Psi^{(2)}\rangle = \sqrt{\frac{2}{3}} \left(\hat{\sigma}_1^{\dagger} \mathcal{S}_2^{\dagger} - \frac{\sqrt{N-1}}{N-2} (\mathcal{S}_2^{\dagger})^2 \right) |G\rangle, \quad (B2)$$

which decays with a rate $(N-2)\Gamma_{1D}$ and is observable in the transmission spectrum. The symmetric single excitation state $|\Psi_{\mathcal{S}}^{(1)}\rangle$ is driven to the symmetric two-excitation Dicke state with the superradiant decay rate $2(N-1)\Gamma_{1D}$. All states shown in Fig. 5 except the symmetric Dicke states $|\Psi_{\mathcal{S}}^{(M)}\rangle$, the ground state $|g\rangle^{\otimes N}$ and the totally inverted state $|e\rangle^{\otimes N}$ are elements of a subspace with degeneracy $d_M = \binom{N}{N-M} - \binom{N}{N-M-1}$. The driving strength (for instance from the single- to

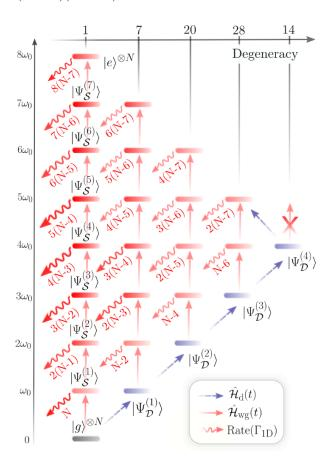


FIG. 5. Energy level diagram for N=8 qubits with multiples of λ_0 separation featuring a coherent drive $\hat{\mathcal{H}}_{\mathrm{d}}(t)$ on individual qubits and a waveguide drive $\hat{\mathcal{H}}_{wg}(t)$ exciting all qubits symmetrically. The symmetric Dicke states $|\Psi_{\mathcal{S}}^{(M)}\rangle$ decay with the superradiant rate $M(N-M+1)\Gamma_{\rm 1D}$ which a maximum at M = N/2. Dark states exist for $M \leq N/2$ and $|\Psi_{\mathcal{D}}^{(M)}\rangle$, which resides in the dark subspace with M excitations, can be efficiently prepared by driving M qubits. The state can be probed via a symmetric waveguide drive on all qubits which excites it into a bright manifold with decay rate $(N-2M)\Gamma_{1D}$. Qubits prepared in the state $|\Psi_{\mathcal{D}}^{(N/2)}\rangle$ lead to complete transmission, as there is no bright manifold above with the same s quantum number. In between symmetric Dicke states and the dark state manifold are bright state manifolds with finite decay rates which are connected by a symmetric excitation to the excitation manifold below. Each subspace has a certain degeneracy which is shown on the top and note that there is no mixing between states from different excitation manifolds due to the absence of collective dephasing (no imperfections).

the two-excitation dark state) is given by

$$\langle \Psi_{\mathcal{D}}^{(2)} | \hat{\mathcal{H}}_{d} | \Psi_{\mathcal{D}}^{(1)} \rangle / \Omega_{d}(t) = \frac{\sqrt{N-3}}{\sqrt{N}} \left(1 + \frac{1}{\sqrt{(N-1)(N-2)}} \right),$$
 (B3)

where the coherent drive only excites the second qubit and the single-excitation dark state has the majority of the excited state population in the first qubit.

Appendix C: Effect of Disorder, Imperfections and Non-Identical Waveguide Couplings

The above results can be generalized to non-identical waveguide couplings, in particular we assume the first qubit is coupled with rate $\Gamma_{1D,1}$ and the remaining qubits with rate $\Gamma_{1D,2}$. Here we show this actually enhances the effect studied so far, that is, an even higher fraction of the excited state population is concentrated in the first qubit and the driving strength of the dark state is equally enhanced. The single-excitation symmetric state can now be written as

$$|\Psi_{\mathcal{S}}^{(1)}\rangle = \frac{1}{\sqrt{\Gamma_{1\mathrm{D},1} + (N-1)\Gamma_{1\mathrm{D},2}}} \left(\sqrt{\Gamma_{1\mathrm{D},1}}\hat{\sigma}_1^{\dagger} + \sqrt{(N-1)\Gamma_{1\mathrm{D},2}}\mathcal{S}_2^{\dagger}\right) |G\rangle,\tag{C1}$$

where the populations in the individual qubits is not equally distributed since the different couplings lead to a redistribution of the excitation. The dark state obtains is readily found to be

$$|\Psi_{\mathcal{D}}^{(1)}\rangle = \frac{1}{\sqrt{\Gamma_{1\mathrm{D},1} + (N-1)\Gamma_{1\mathrm{D},2}}} \left(\sqrt{(N-1)\Gamma_{1\mathrm{D},2}}\hat{\sigma}_1^{\dagger} - \sqrt{\Gamma_{1\mathrm{D},1}}\mathcal{S}_2^{\dagger}\right) |G\rangle. \tag{C2}$$

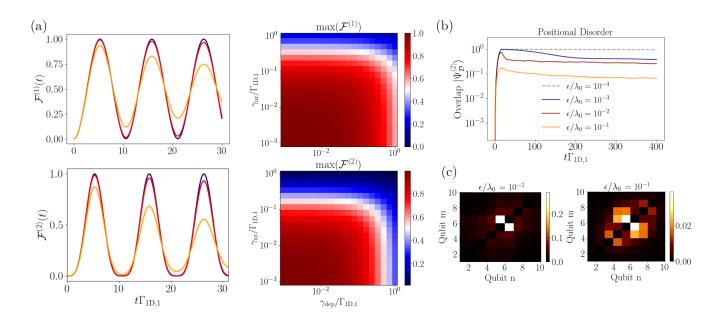


FIG. 6. (a) Dark state preparation under dephasing and non-radiative decay for N=6 qubits with $\Gamma_{1\mathrm{D},2}=20\Gamma_{1\mathrm{D},1}$ for either the last 4 or last 5 qubits and $d=\lambda_0$ and under continuous driving with Rabi frequency $\Omega_{\rm d}/\Gamma_{1\mathrm{D},1}=0.3$ for either the first or the first two qubits. The time evolution of the fidelity with the target state $\mathcal{F}^{(M)}(t)=|\langle\Psi^{(M)}_{\mathcal{D}}|\rho(t)|\Psi^{(M)}_{\mathcal{D}}\rangle|^2$ is shown. Blue, red and orange lines correspond to dephasing rates (i) $\gamma_d=0$, (ii) $\gamma_d=0.01\Gamma_{1\mathrm{D},1}$, (iii) $\gamma_d=0.1\Gamma_{1\mathrm{D},1}$ respectively, with $\gamma_{\rm nr}=0$. Also shown is the maximal fidelity for preparing the one- or two-excitation dark state $|\Psi^{(M)}_{\mathcal{D}}\rangle$ in the presence of non-radiative loss and dephasing rates γ_d and $\gamma_{\rm nr}$. (b) Influence of classical position disorder ϵ/λ_0 on the two-excitation dark state preparation with a rectangular driving pulse on the central two qubits and decay rate in a chain of N=10 qubits. The disorder is assumed to be following a normal distribution of standard deviation ϵ and 200 random configurations for each value of ϵ are considered. (c) The averaged spatial correlation $|\langle e_n e_m | \Psi(t) \rangle|^2$ is shown at $t\Gamma_{1\rm D}=20$ for the disordered arrays in (b).

The amount of population in the first qubit for the dark state is given by $(N-1)\Gamma_{1D,2}/(\Gamma_{1D,1}+(N-1)\Gamma_{1D,2})$ and in particular for $\Gamma_{1D,2} \gg \Gamma_{1D,1}$ most is stored in the first qubit even for small N. It follows that the dark state can be prepared even more efficiently given that $\Gamma_{1D,1} < \Gamma_{1D,2}$.

The two-excitation dark state, with the first two qubits having a coupling rate $\Gamma_{1D,1}$, is given by

$$|\Psi_{\mathcal{D}}^{(2)}\rangle = \frac{1}{\sqrt{\alpha}} \left(\frac{\sqrt{\Gamma_{\text{1D},1}\Gamma_{\text{1D},2}}}{\Gamma_{\text{1D},1}} (\mathcal{S}_1^{\dagger})^2 + \frac{\sqrt{\Gamma_{\text{1D},1}\Gamma_{\text{1D},2}}}{\Gamma_{\text{1D},2}(N-2)} (\mathcal{S}_2^{\dagger})^2 - \frac{\sqrt{2}}{\sqrt{N-1}} \mathcal{S}_1^{\dagger} \mathcal{S}_2^{\dagger} \right) |G\rangle, \tag{C3}$$

with

$$\alpha = \frac{\Gamma_{1D,2}^2(N-1)(N-2) + 2\Gamma_{1D,1}\Gamma_{1D,2}(N-2) + 2\Gamma_{1D,1}^2}{\Gamma_{1D,1}\Gamma_{1D,2}(N-2)}.$$
 (C4)

In a realistic scenario both dephasing and excitation loss into channels other than the waveguide are present and affect the fidelities of driving the one- and two-excitation dark state as well as their lifetimes. The non-waveguide decay and dephasing are included as uncorrelated terms in the Lindbladian and the master equation for arbitrary distances obtains the form

$$\dot{\hat{\rho}} = -i[\hat{\mathcal{H}}_{\text{eff}}, \hat{\rho}] + \sum_{m,n} \Gamma_{m,n} \hat{\sigma}_m \hat{\rho} \hat{\sigma}_n^{\dagger} + \gamma_{\text{nr}} \sum_{m} \hat{\sigma}_m \hat{\rho} \hat{\sigma}_m^{\dagger} + 2\gamma_{\text{dep}} \sum_{m} \hat{\sigma}_m^{\dagger} \hat{\sigma}_m \hat{\rho} \hat{\sigma}_m^{\dagger} \hat{\sigma}_m, \tag{C5}$$

and the effective Hamiltonian in the interaction picture is given by

$$\hat{\mathcal{H}}_{\text{eff}} = \sum_{m,n} \left(J_{m,n} - i \frac{\Gamma_{m,n}}{2} \right) \hat{\sigma}_m^{\dagger} \hat{\sigma}_n - i \frac{\gamma_{\text{nr}} + 2\gamma_{\text{dep}}}{2} \sum_m \hat{\sigma}_m^{\dagger} \hat{\sigma}_m.$$
 (C6)

For instance in Fig. 6(a) the influence of individual qubit dephasing and non-radiative decay on the dark state preparation fidelity is shown for non-identical waveguide couplings. A high preparation fidelity is prevailing even under considerable individual dephasing and decay, which in state-of-the-art laboratories working with superconducting qubits can be held below $10^{-2}\Gamma_{1D,1}$ for both. In Fig. 6(b) the two-excitation dark state preparation and decay rate are shown for various degrees of classical position disorder. Each qubit is randomly displaced around its multiple of λ_0 position by a normal distribution of standard deviation ϵ . The overlap with $|\Psi_{\mathcal{D}}^{(2)}\rangle$ is plotted after performing an average over disorder realizations which is confined along the 1D chain axis. The number of disorder realizations is 200 and in Fig. 6(c) the averaged spatial correlation $|\langle e_n e_m | \Psi(t) \rangle|^2$ is shown after the overlap reached the maximum value. For quantum platforms in the microwave regime e.g. superconducting transmon qubits, the positional disorder can be kept well below 10^{-4} but even other platforms like atoms trapped along a nanofiber exhibit small positional disorder.

Appendix D: Multilevel Nature of the Transmon Qubit

For the specific platform of superconducting transmon qubits the involved quantum emitters are inherently anharmonic and due to the multilevel nature it is necessary to model each emitter as a multilevel quantum emitter to capture the full richness of possible quantum states. So far we assumed a large enough anharmonicity U between the first and second excited state in each transmon and therefore neglected the second excited state to recover the two-level qubit. Here we show that the results obtained above still prevail in the case of small U and even the harmonic oscillator case U = 0. Let us first begin to write down the effective Hamiltonian for N transmons, which is given by

$$\hat{\mathcal{H}}_{\text{eff}} = \sum_{m,n} \left(J_{m,n} - i \frac{\Gamma_{m,n}}{2} \right) \hat{a}_m^{\dagger} \hat{a}_n - \frac{U}{2} \sum_m \hat{n}_m (\hat{n}_m - \mathbb{I}), \tag{D1}$$

whereas the Lindbladian retains the same form as in the qubit case. The bosonic operator \hat{a}_m^{\dagger} creates an excitation on the site m and \hat{n}_j is the number operator of the site m. For many-body dynamics the anharmonicity U serves as an on-site interaction and the weaker the anharmonicity, the closer the system resembles the harmonic oscillator. For arbitrary U the transmons generally behave like anharmonic oscillators but assuming only a single excitation is present in the system, the single-excitation dark and bright states have the same form as in the qubit case with the exchange $\hat{\sigma}_m \leftrightarrow \hat{a}_m$. The completely symmetric state with two excitations can be written as

$$|\Phi_{\mathcal{S}}^{(2)}\rangle = \frac{\sqrt{2}}{N} \sum_{n,m} \hat{a}_n^{\dagger} \hat{a}_m^{\dagger} |G\rangle = \frac{\sqrt{2}}{N} \Big((\hat{a}_1^{\dagger})^2 + \sqrt{N-1} \hat{a}_1^{\dagger} \mathcal{S}_2^{\dagger} + (N-1) (\mathcal{S}_2^{\dagger})^2 \Big) |G\rangle, \tag{D2}$$

with the superradiant decay rate $2N\Gamma_{1D}$ which is larger than the superradiant rate of the two-excitation symmetric Dicke state. The two-excitation dark state with two excitations per site and the majority of the excitation in the first transmon is given by

$$|\Phi_{\mathcal{D}}^{(2)}\rangle = \frac{\sqrt{2}}{N} \Big((\hat{a}_1^{\dagger})^2 - 2\sqrt{N - 1}\hat{a}_1^{\dagger} \mathcal{S}_2^{\dagger} + (\mathcal{S}_2^{\dagger})^2 \Big) |G\rangle, \tag{D3}$$

with the fraction 2(N-1)/N of the population in the first transmon and $N \geq 2$. As before, any transmon is equally valid to store the majority of the population and which one is determined whether or not it is excited by an external drive. The other possible dark state involving superpositions of symmetric states in the sub-arrays is equivalent to the two-excitation dark state for the qubit case $|\Psi_{\mathcal{D}}^{(2)}\rangle$ with the exchange $\hat{\sigma}_m^{\dagger} \leftrightarrow \hat{a}_m^{\dagger}$ in \mathcal{S}_1^{\dagger} and \mathcal{S}_2^{\dagger} respectively. Assuming that the first two transmons are driven by an external drive, the general dark state for arbitrary anharmonicities U is a superposition of the aforementioned dark states, namely $c_1|\Psi_{\mathcal{D}}^{(2)}\rangle+c_2|\Phi_{\mathcal{D}}^{(2)}\rangle$. Notably, the state $|\Phi_{\mathcal{D}}^{(2)}\rangle$ acquires a energy shift as well coming from the onsite interaction term in the Hamiltonian and has to be taking into account while driving the quibts externally. This shows that the effect described for the qubit case extends to the transmonic regime with the collective dark and bright states having a slightly modified distribution in the populations due to their multilevel structure. Typical values for the anharmonicity are $U \sim 200-300$ MHz whereas the waveguide decay rate Γ_{1D} is in the range of 1-100 MHz.